

We are IntechOpen, the world's leading publisher of Open Access books Built by scientists, for scientists

6,900

Open access books available

186,000

International authors and editors

200M

Downloads

Our authors are among the

154

Countries delivered to

TOP 1%

most cited scientists

12.2%

Contributors from top 500 universities



WEB OF SCIENCE™

Selection of our books indexed in the Book Citation Index
in Web of Science™ Core Collection (BKCI)

Interested in publishing with us?
Contact book.department@intechopen.com

Numbers displayed above are based on latest data collected.
For more information visit www.intechopen.com



Investigations of Phonons in Zinc Blende and Wurtzite by Raman Spectroscopy

Lin Sun, Lingcong Shi and Chunrui Wang

Additional information is available at the end of the chapter

<http://dx.doi.org/10.5772/64194>

Abstract

The importance of phonons and their interactions in bulk materials is well known to those working in the fields of solid-state physics, solid-state electronics, optoelectronics, heat transport, quantum electronic, and superconductivity. Phonons in nanostructures may act as a guide to research on dimensionally confined phonons and lead to phonon effects in nanostructures and phonon engineering. In this chapter, we introduce phonons in zinc blende and wurtzite nanocrystals. First, the basic structure of zinc blende and wurtzite is described. Then, phase transformation between zinc blende and wurtzite is presented. The linear chain model of a one-dimensional diatomic crystal and macroscopic models are also discussed. Basic properties of phonons in wurtzite structure will be considered as well as Raman mode in zinc blende and wurtzite structure. Finally, phonons in ZnSe, Ge, SnS₂, MoS₂, and Cu₂ZnSnS₄ nanocrystals are discussed on the basis of the above theory.

Keywords: phonons, zinc blende, wurtzite, Raman spectroscopy, molecular vibration

1. Zinc blende and wurtzite structure

Crystals with cubic/hexagonal structure are of major importance in the fields of electronics and optoelectronics. Zinc blende is typical face-centered cubic structure, such as Si, Ge, GaAs, and ZnSe. Wurtzite is typical hexagonal close packed structure, such as GaN and ZnSe. In particular, II–VI or III–V group semiconductor nanowires always coexist two structures, one cubic form with zinc blende (ZB) and another hexagonal form with wurtzite (WZ) structure. Sometimes, this coexistence between zinc blende and wurtzite structure leads to form twinning crystal during the phase transformation between zinc blende and wurtzite [1, 2].

1.1. Basic structure of zinc blende and wurtzite

The crystal structure of zinc selenide in the zinc blende structures is shown in **Figure 1**, which is regarded as two face-centered cubic (fcc) lattices displaced relative to each other by a vector $\frac{a}{4}\vec{i} + \frac{a}{4}\vec{j} + \frac{a}{4}\vec{k}$, where a is lattice constant. Close-packed planes of zinc blende are $\{111\}$ along $\langle 111 \rangle$, and the stacking is ...ABCABCA...; the adjacent plane separation is $\sqrt{3}/3a$. Along $\langle 100 \rangle$, the stacking is ...ABABAB...; the adjacent plane separation is $a/2$. Along $\langle 110 \rangle$, the stacking is ...ABABABA...; the adjacent plane separation is $\sqrt{2}/4a$. Zinc blende structures have eight atoms per unit cell.

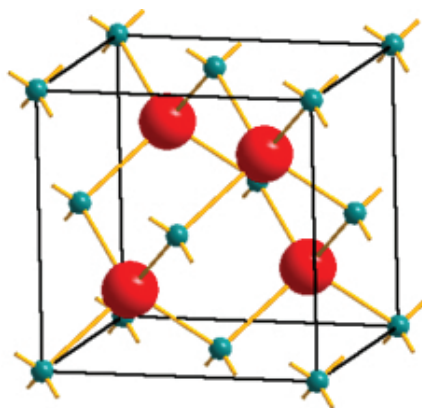


Figure 1. Zinc blende crystal structure.

Figure 2 is wurtzite structure of zinc selenium. Close-packed planes of wurtzite are $\{0001\}$ along $\langle 0001 \rangle$, and the stacking is ...ABABA... Adjacent plane spacing is $c/2$. Wurtzite structures have four atoms per unit cell. In zinc blende, the bonding is tetrahedral. The wurtzite structure may be generated from zinc blende by rotating adjacent tetrahedra about their common bonding axis by an angle of 60° with respect to each other.

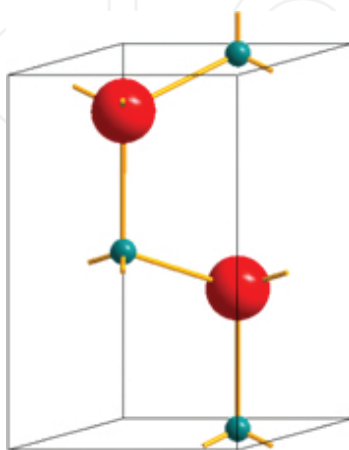


Figure 2. Wurtzite crystal structure.

1.2. Phase transformation between zinc blende and wurtzite

Research into controlling nanowire crystal structure has intensified. Several reports address the diameter dependency of nanowire crystal structure, with smaller diameter nanowires tending toward a WZ phase and larger diameter nanowires tending toward a ZB phase. Allowing for ZnSe, two phases, zinc blende (ZB) and wurtzite (WZ), exist, and the (111) faces of ZB phase are indistinguishable from and match up with the (001) faces of WZ phase, the subtle structural differences of which lead to the attendant small difference in the internal energies (~ 5.3 meV/atom for ZnSe). The WZ-ZB phase transformation is considered to be caused by the crystal plane slip. Take the formation of ZnSe longitudinal twinning nanowires, for example [3]. Structurally, the (001) planes of WZ and the (111) planes of ZB are their corresponding close packing planes. ABAB stacking for WZ and ABCABC stacking for ZB are shown in **Figure 3a** and **b**, respectively. It was noteworthy that the arrangement of atoms in A/B packing planes was different in WZ phase. So the phase transition could not be realized until the smaller Zn atoms moved to the interspaces provided by three neighboring bigger Se atoms, within the plane B. In this case, the new layers B' were obtained, and then, the slip occurs between neighboring planes A and B' by $\frac{1}{3}\vec{a} + \frac{2}{3}\vec{b}$, that is $\langle 120 \rangle$ direction, indicated in **Figure 3a**.

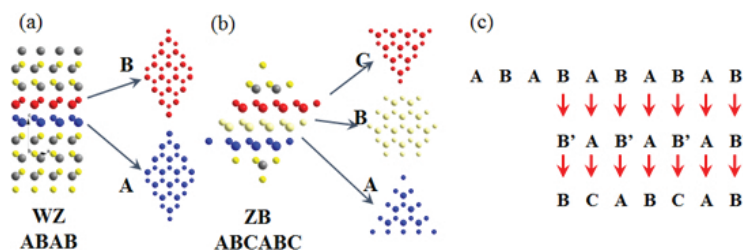


Figure 3. Phase transformation between zinc blende and wurtzite. (a) The arrangement of atoms in WZ phase; (b) The arrangement of atoms in ZB phase; (Se is shown with the bigger sphere and Zn is shown in little one.) (c) The stacking sequence schematic model showing the phase transformation process from WZ phase to ZB phase.

Generally, there are three equivalent directions to realized the slip, which are $\langle 120 \rangle$, $\langle \bar{2}\bar{1}0 \rangle$, and $\langle 1\bar{1}0 \rangle$. Such a displacement could be indicated in **Figure 3c**, and the ZB structure could be obtained through the slip between every second close-packed layer in the WZ sequence to form the ABC stacking.

2. Linear-chain model and macroscopic models

To the simple double lattice, lattice vibration can be described by the one-dimensional diatomic model. The linear-chain model of a diatomic crystal is based upon a system of two atoms with masses, m and M , placed along a one-dimensional chain as depicted in **Figure 4**. The separation between the atomics is " a ", and the vibration in the vicinity of their equilibrium position is treated as the simple harmonic vibration. The properties of optical phonon can be described

based on the macroscopic fields. It is the model based on the Huang and Maxwell equations, which has great utility in describing the phonons in the uniaxial crystals such as wurtzite crystals.

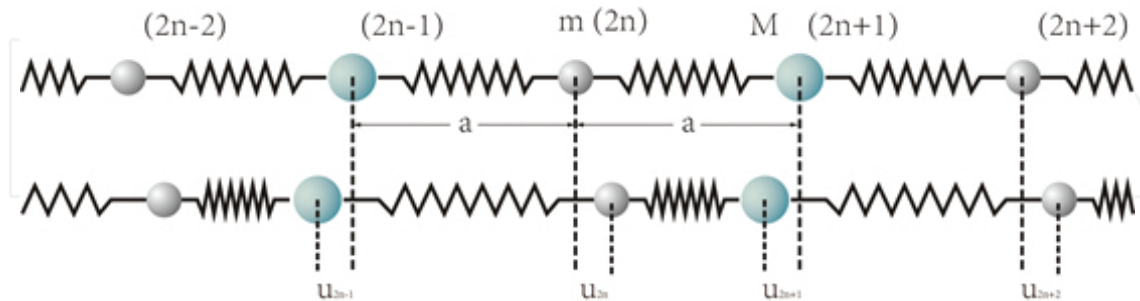


Figure 4. One-dimensional diatomic linear-chain model.

2.1. Polar semiconductors

Polar semiconductor is the crystal that consists of different ions. In polar semiconductor, the lattice vibration is associated with the electric dipole moment and electric field generation. Assume that the vibration frequency is ω , wave vector is \vec{q} , then the intensity of polarization can be written as follows,

$$\vec{P} = \vec{P}_0 e^{i(\omega t - \vec{q} \cdot \vec{r})} \quad (2-1)$$

Solve the simultaneous formula (2-1) and Maxwell equations can obtain,

$$\vec{E} = \frac{\omega^2 \vec{P} - \vec{q} c^2 (\vec{q} \cdot \vec{P})}{\epsilon_0 (q^2 c^2 - \omega^2)} \quad (2-2)$$

To longitudinal polarity lattice mode, $\vec{p} // \vec{q}$, formula (2-2) can be simplified as follows,

$$\vec{E}_L = -\frac{\vec{P}}{\epsilon_0} \quad (2-3)$$

To transverse polarity lattice mode, $\vec{p} \perp \vec{q}$, formula (2-2) can be simplified as follows,

$$\vec{E}_T = \frac{\omega^2}{\epsilon_0 (q^2 c^2 - \omega^2)} \vec{P} \quad (2-4)$$

As was apparent above, polar optical phonon vibrations produce electric fields and electric polarization fields that may be described in terms of Maxwell's equations and the driven-oscillator equations. Assume that the mass of the ions are M_+ , M_- , the charges are $\pm Ze$, displacements are u_{\pm} , the force constant is k ,

$$M_+ \ddot{u}_+ = -k\bar{u} + Ze\vec{E}_e \quad (2-5)$$

$$M_- \ddot{u}_- = k\bar{u} - Ze\vec{E}_e \quad (2-6)$$

where \vec{E}_e is the effect electric field, $\vec{u} = \vec{u}_+ - \vec{u}_-$, then

$$\bar{M}\ddot{\bar{u}} = -k\bar{u} + Ze\vec{E}_e \quad (2-7)$$

where $\bar{M} = \frac{M_+ M_-}{M_+ + M_-}$ is reduced mass.

The lattice vibration is associated with the electric dipole moment generation, which can be described as follows,

$$\vec{P} = \frac{1}{\Omega}(Ze\vec{u} + \alpha\vec{E}_e) \quad (2-8)$$

where Ω is the volume of the primitive cell, and α is the electron polarization. Under the effective field approximation, the effective field can be described as follows,

$$\vec{E}_e = \vec{E} + \frac{\vec{P}}{3\epsilon_0} \quad (2-9)$$

Replace the value of \vec{P} in formula (2-9) with (2-8),

$$\vec{E}_e = \frac{3\epsilon_0\Omega\vec{E} + Ze\vec{u}}{3\epsilon_0\Omega - \alpha} \quad (2-10)$$

Then, take formula (2-7) and (2-9) into (2-10),

$$\ddot{\bar{u}} = A\bar{u} + B\vec{E} \quad (2-11)$$

$$\vec{P} = C\vec{E} + D\vec{u} \quad (2-12)$$

where

$$A = -\frac{k}{M} + \frac{Z^2 e^2}{M(3\varepsilon_0 \Omega - \alpha)} \quad (2-13)$$

$$B = \frac{3\varepsilon_0 \Omega Z e}{M(3\varepsilon_0 \Omega - \alpha)} \quad (2-14)$$

$$C = \frac{3\varepsilon_0 \alpha}{3\varepsilon_0 \Omega - \alpha} \quad (2-15)$$

$$D = \frac{3\varepsilon_0 Z e}{3\varepsilon_0 \Omega - \alpha} \quad (2-16)$$

formula (2-11) and (2-12) are the Huang equations, which are the basic equations of describing the vibrations of long wave in the polar crystals. From the formula (2-14) and (2-16), one can find that,

$$B = \frac{\Omega}{M} D \quad (2-17)$$

When the system is under the high-frequency electric field, formula (2-12) reduces to

$$\vec{P} = C\vec{E} \quad (2-18)$$

For $\varepsilon(\infty) = 1 + \frac{\vec{P}}{\varepsilon_0 \vec{E}}$, formula (2-18) can be written as follows,

$$C = \varepsilon_0 [\varepsilon(\infty) - 1] \quad (2-19)$$

Compute the curl of formula (2-11) and solve the simultaneous equations of (2-12) and electrostatic equations $\nabla \times \vec{E} = 0$,

$$A = -\omega_0^2 \quad (2-20)$$

When the system is under the static electric field, $\ddot{u} = 0$, and formula (2-11) reduces to

$$\vec{u} = -\frac{B}{A}\vec{E} \quad (2-21)$$

Take formula (2-21) into (2-12),

$$\vec{P} = \left(C - \frac{BD}{A}\right)\vec{E} \quad (2-22)$$

Replace the electrostatic equation,

$$\vec{P} = [\varepsilon(0) - 1]\varepsilon_0\vec{E} \quad (2-23)$$

And take formula (2-23) and (2-20) into (2-22),

$$BD = [\varepsilon(0) - \varepsilon(\infty)]\varepsilon_0\omega_0^2 \quad (2-24)$$

Solve the simultaneous equations of (2-17) and (2-24) can obtain

$$B = \left(\frac{\Omega}{\bar{M}}\right)^{\frac{1}{2}} \{[\varepsilon(0) - \varepsilon(\infty)]\varepsilon_0\}^{\frac{1}{2}} \omega_0 \quad (2-25)$$

$$D = \left(\frac{\bar{M}}{\Omega}\right)^{\frac{1}{2}} \{[\varepsilon(0) - \varepsilon(\infty)]\varepsilon_0\}^{\frac{1}{2}} \omega_0 \quad (2-26)$$

Solve two simultaneous Maxwell and Huang equations,

$$\nabla \times \vec{E} = -\mu_0 \frac{\partial \vec{H}}{\partial t} \quad (2-27a)$$

$$\nabla \times \vec{H} = \frac{\partial}{\partial t} (\varepsilon_0 \vec{E} + \vec{P}) \quad (2-27b)$$

$$\nabla \cdot \vec{D} = 0 \quad (2-27c)$$

$$\nabla \cdot \vec{H} = 0 \quad (2-27d)$$

Assume the solution forms are

$$\vec{u} = \vec{u}_0 e^{i(q \cdot r - \omega t)} \quad (2-28a)$$

$$\vec{P} = \vec{P}_0 e^{i(q \cdot r - \omega t)} \quad (2-28b)$$

$$\vec{E} = \vec{E}_0 e^{i(q \cdot r - \omega t)} \quad (2-28c)$$

$$\vec{H} = \vec{H}_0 e^{i(q \cdot r - \omega t)} \quad (2-28d)$$

Take (2-28) into the Huang and Maxwell equations,

$$\vec{P}_0 = \left[-\frac{BD}{A + \omega^2} + C \right] \vec{E}_0 \quad (2-29)$$

$$(\vec{q} \cdot \vec{E}_0) \left[\varepsilon_0 + C - \frac{BD}{A + \omega^2} \right] = 0 \quad (2-30)$$

To the longitudinal wave, $\vec{q} \cdot \vec{E}_0 \neq 0$, (2-30) reduces to

$$\varepsilon_0 + C - \frac{BD}{A + \omega^2} = 0 \quad (2-31)$$

Take (2-19) (2-20) (2-25) (2-26) into (2-31)

$$\omega_{LO}^2 = \frac{\varepsilon(0)}{\varepsilon(\infty)} \omega_0^2 \quad (2-32)$$

Equation (2-23) is the dispersion relations of longitudinal wave, which is commonly called Lyddane-Sachs-Teller (LST) relationship. LST relation indicates that the frequency of longitudinal wave is a constant and independent on the wave vector.

Similarly, to the transverse wave, $\vec{q} \cdot \vec{E}_0 = 0$, solve the simultaneous equations of Maxwell and Huang equations,

$$\frac{q^2}{\mu_0 \omega} = \omega \left(\varepsilon_0 + C - \frac{BD}{A + \omega^2} \right) \quad (2-33)$$

Replace the values of A , B , C , and D into (2-33),

$$\frac{c^2}{\omega^2} q^2 = \varepsilon(\infty) + \frac{\varepsilon(0) - \varepsilon(\infty)}{\omega_0^2 - \omega^2} \omega_0^2 \quad (2-34)$$

Equation (2-34) is the dispersion relations of transverse wave. One can find that the frequency of transverse is dependent on the value of wave vector \vec{q} , but independent on its direction [4, 5].

2.2. Dispersion relations

One-dimensional diatomic model can be regarded as the simple double lattice. In the simple linear chain model, it is assumed that only nearest neighbors are coupled, and that the interaction between these atoms is described by Hooke's law; the spring constant α is taken to be that of a harmonic oscillator. Thus, the kinematical equations are established,

$$m\ddot{\vec{u}}_{2n} = -\beta(2\ddot{\vec{u}}_{2n} - \ddot{\vec{u}}_{2n+1} - \ddot{\vec{u}}_{2n-1}) \quad (2-35a)$$

$$M\ddot{\vec{u}}_{2n+1} = -\beta(2\ddot{\vec{u}}_{2n+1} - \ddot{\vec{u}}_{2n+2} - \ddot{\vec{u}}_{2n}) \quad (2-35b)$$

where m and M are the mass of the adjacent atoms and \vec{u}_{2n-1} , \vec{u}_{2n} , \vec{u}_{2n+1} , and \vec{u}_{2n+2} are the displacements of the atoms at the position of $2n-1$, $2n$, $2n+1$, and $2n+2$, respectively. β is the force constant. The solution forms of (2-35) can be written as follows

$$\vec{u}_{2n} = A_1 e^{i[(\omega t - (2n)\vec{a} \cdot \vec{q})]} \quad (2-36a)$$

$$\vec{u}_{2n+1} = A_2 e^{i[(\omega t - (2n+1)\vec{a} \cdot \vec{q})]} \quad (2-36b)$$

where \vec{q} is the phonon wave vector and ω is its frequency. Take formulas (2-36a) and (2-36b) into formulas (2-35a) and (2-35b),

$$-m\omega^2 A_1 = \beta(e^{-i\vec{a} \cdot \vec{q}} + e^{i\vec{a} \cdot \vec{q}})A_2 - 2\beta A_1 \quad (2-37)$$

$$-M\omega^2 A_2 = \beta(e^{-i\vec{a} \cdot \vec{q}} + e^{i\vec{a} \cdot \vec{q}})A_1 - 2\beta A_2 \quad (2-38)$$

Eliminating A_1 and A_2 ,

$$\omega^2 = \beta \frac{M+m}{Mm} \left\{ 1 \pm \left[1 - \frac{4Mm}{(M+m)^2} \sin^2(\bar{a} \cdot \bar{q}) \right]^{1/2} \right\} \quad (2-39)$$

The relationship between frequency and wave vector is commonly called dispersion relation [5].

3. Basic properties of phonons in wurtzite structure

In this section, we discuss the phonon effects in wurtzite structure. The crystalline structure of a wurtzite material is depicted in **Figure 2**. There are four atoms in the unit cell. Thus, the total number of optical modes in the long-wavelength limit is nine: three longitudinal optic (LO) and six transverse optic (TO). In these optical modes, there are only three polar optical vibration modes. According to the group theory, the wurtzite crystal structure belongs to the space group C_{6v}^4 and the phonon modes at Γ point of the Brillouin zone are represented by the following irreducible representations:

$$\Gamma = 2A_1 + 2B + 2E_1 + 2E_2$$

Due to the anisotropy of wurtzite structure, the vibrational frequency of oscillates parallel and perpendicular to the optical axis is denoted by ω_{eT} and ω_{oT} , and the corresponding dielectric constants are denoted by ϵ_{es} , $\epsilon_{e\infty}$ and ϵ_{os} , $\epsilon_{o\infty}$. The corresponding components can be written as the form of Huang equations, and the dispersion relation can be obtained by solving two simultaneous equations of Maxwell and Huang equations.

$$\frac{q^2 c^2}{\omega^2} = \epsilon_0 = \frac{\omega_{oT}^2 \epsilon_{os} - \omega^2 \epsilon_{o\infty}}{\omega_{oT}^2 - \omega^2} \quad (3-1)$$

$$\frac{q^2 c^2}{\omega^2} = \epsilon_\theta = \frac{\left(\frac{\omega_{eT}^2 \epsilon_{es} - \omega^2 \epsilon_{e\infty}}{\omega_{eT}^2 - \omega^2} \right) \left(\frac{\omega_{oT}^2 \epsilon_{os} - \omega^2 \epsilon_{o\infty}}{\omega_{oT}^2 - \omega^2} \right)}{\left(\frac{\omega_{eT}^2 \epsilon_{es} - \omega^2 \epsilon_{e\infty}}{\omega_{eT}^2 - \omega^2} \right) \cos^2 \theta + \left(\frac{\omega_{oT}^2 \epsilon_{os} - \omega^2 \epsilon_{o\infty}}{\omega_{oT}^2 - \omega^2} \right) \sin^2 \theta} \quad (3-2)$$

where ϵ_0 and ϵ_θ is the dielectric constants of ordinary and extraordinary wave, is the included angle between wave vector and optical axis.

When the wave vector is parallel to the optical axis, $\theta = 0$, formula (3-2) reduce to

$$\varepsilon_{\theta} = \frac{\omega_{oT}^2 \varepsilon_{os} - \omega^2 \varepsilon_{o\infty}}{\omega_{oT}^2 - \omega^2} \quad (3-3)$$

which is the same as formula (3-1). When the wave vector is perpendicular to the optical axis, $\theta = 90^\circ$, formula (3-2) reduces to

$$\varepsilon_{\theta} = \frac{\omega_{eT}^2 \varepsilon_{es} - \omega^2 \varepsilon_{o\infty}}{\omega_{eT}^2 - \omega^2} \quad (3-4)$$

Formula (3-4) indicates that the extraordinary wave is transverse wave when the wave vector is perpendicular to the optical axis.

When $q \gg \omega/c$, formulas (3-1) and (3-2) can be rewritten as follows,

$$\omega = \omega_{oT} \quad (3-5)$$

and

$$\left(\frac{\omega_{eT}^2 \varepsilon_{es} - \omega^2 \varepsilon_{e\infty}}{\omega_{eT}^2 - \omega^2}\right) \cos^2 \theta + \left(\frac{\omega_{oT}^2 \varepsilon_{os} - \omega^2 \varepsilon_{o\infty}}{\omega_{oT}^2 - \omega^2}\right) \sin^2 \theta = 0 \quad (3-6)$$

Formula (3-5) indicates that frequency of ordinary phonon is independent on the wave vector q . Formula (3-6) indicates that the frequency of extraordinary phonon is dependent on the orientation of the wave vector, but independent on its value.

It is most convenient to divide uniaxial crystals into two categories: (a) the electrostatic forces dominate over the anisotropy of the interatomic forces and (b) the short-range interatomic forces are much greater than the electrostatic forces. It has been turned out that crystals with the wurtzite symmetry fall into the first category. In this case, $|\omega_{eT} - \omega_{oT}| \ll |\omega_{eL} - \omega_{oT}|$ and $|\omega_{oL} - \omega_{oT}|, \varepsilon_{e\infty} \approx \varepsilon_{o\infty} = \varepsilon_{\infty}$, formula (3-5) reduces to

$$\left(\frac{\omega_{eL}^2 - \omega^2}{\omega_{eT}^2 - \omega^2}\right) \cos^2 \theta + \left(\frac{\omega_{oL}^2 - \omega^2}{\omega_{oT}^2 - \omega^2}\right) \sin^2 \theta = 0 \quad (3-7)$$

thus,

$$\omega^2 \approx \omega_{eT}^2 \sin^2 \theta + \omega_{oT}^2 \cos^2 \theta \quad (3-8)$$

and

$$\omega^2 \approx \omega_{oL}^2 \sin^2 \theta + \omega_{oT}^2 \cos^2 \theta \quad (3-9)$$

4. Raman mode in zinc blende and wurtzite structure

Raman spectroscopy is a non-destructive technical tool used to gain information about the phonon behavior of the crystal lattice through the frequency shift of the inelastically scattered light from the near surface of the sample. It is well known that different crystal phases have different vibrational behaviors, so the measured Raman shifts of different phases are mostly unique and can be seen as fingerprints for the respective phases. This provides the possibility of detecting different phases in a sample. It has been developed to be a versatile tool for the characterization of semiconductors leading to detailed information on crystal structure, phonon dispersion, electronic states, composition, strain, and so on of semiconductor nanostructures.

In a zinc blende structure, the space group of the cubic unit cell is $F43m(T_d^2)$ containing four formula units. The primitive unit cell contains only one formula per unit cell, and hence, there are three optical branches to the phonon dispersion curves. As there is no center of inversion in the unit cell, the zone-center transverse optic (TO) and longitudinal optic (LO) optic modes are Raman active. The optic mode is polar so that the macroscopic field lifts the degeneracy, producing a non-degenerate longitudinal mode that is at a higher frequency than the two transverse modes.

The wurtzite crystal structure belongs to the space group C_{6v}^4 and group theory predicts zone-center optical modes are A_1 , $2B_1$, E_1 , and $2E_2$. The A_1 and E_1 modes and the two E_2 modes are Raman active, whereas the B modes are silent. The A and E modes are polar, resulting in a splitting of the LO and the TO modes [6].

5. Phonons in ZnSe, Ge, SnS₂, MoS₂, and Cu₂ZnSnS₄ nanocrystals

In addition to the attached references, this chapter is primarily written on the basis of our research works. Here, we select ZnSe, Ge nanowires and CdSe/Ge-based nanowire heterostructures, two-dimensional semiconductors SnS₂ and MoS₂, and candidate absorber materials of thin-film solar cells Cu₂ZnSnS₄. These examples will help us to understand the phonons behaviors in nanostructures.

It is well known that ZnSe has two structures: cubic zinc blende (ZB) and hexagonal wurtzite (WZ) due to the difference of the stacking sequence of successive layers, whereas Ge has diamond structure. SnS₂ and MoS₂ belong to the wide family of compounds with layered

structures. SnS_2 crystal is isostructural to the hexagonal CdI_2 -type structure. MoS_2 usually consists of a mixture of two major polytypes of similar structure, 2H (hexagonal) and 3R (rhombohedral), with the former being more abundant. As for quaternary $\text{Cu}_2\text{ZnSnS}_4$ (CZTS), the parent binary II-VI semiconductors adopt the cubic zinc blende structure, and the ternary I-III-VI₂ compounds can be generated by mutating the group II atoms into pairs of group I and III atoms. The quaternary CZTS materials are formed by replacing the two In (III) atoms with Zn (II) and Sn (IV), respectively (see Figure 5).

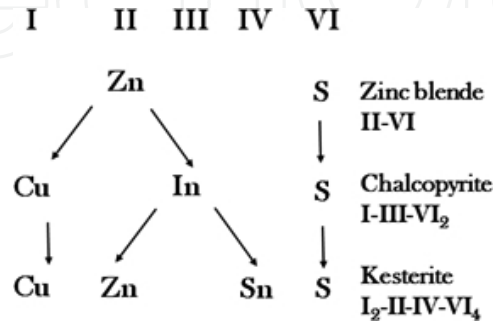


Figure 5. Evolution of multinary compounds.

We use Raman spectroscopy to identify crystal structure of ZnSe one-dimensional material (Figure 6). In sample S3, the Raman peaks at 204 and 251 cm^{-1} are attributed to the scatterings of the transverse optic (TO) and longitudinal optic (LO) phonon modes of ZnSe, respectively. A strong peak at 232 cm^{-1} , between the TO and LO phonons, is thought to be surface mode. The Raman peak at $\sim 176 \text{ cm}^{-1}$ is attributed to the hexagonal phase $E_1(\text{TO})$ mode of ZnSe, which is inhibited in Raman spectrum (RS) of ZB ZnSe. Compared with S3, Raman peaks at 205.6 (TO mode) and 252 cm^{-1} (LO mode) of S1 show tiny blue-shift. However, in S1, there is no Raman peak corresponding to the surface mode, as well as $E_1(\text{TO})$ mode, which is suppressed in the

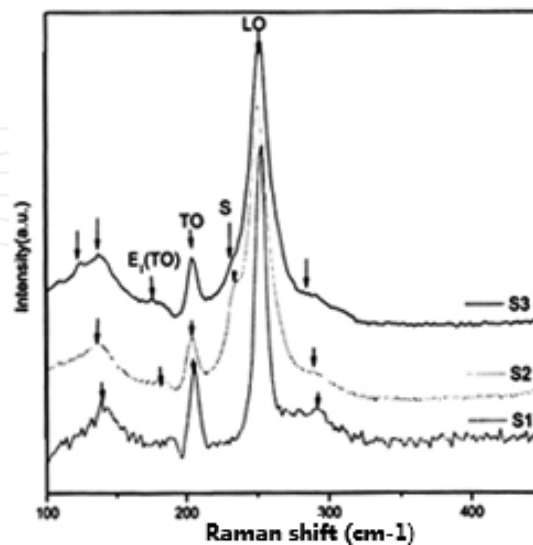


Figure 6. Room temperature Raman spectra of ZnSe. S1, S2, and S3 stand for ZB, coexist of ZB and WZ, WZ ZnSe nanostructure.

ZB phase. This indicates the existence of ZB phase in S1. Thus, structure of the sample can be shown through RS, and we got S1-ZB phase, S3-WZ, S2 the coexist of ZB and WZ [7] (cm^{-1}).

Figure 7 shows the room temperature RS of CdSe/Ge-based nanowires. The LO mode of Ge in CdSe-Ge (or CdSe-Ge-CdSe), -CdSe-Ge core/polycrystalline Ge sheath, and -Ge-GeSe heterostructural nanowires has a downshift by 8, 5, and 2 cm^{-1} in comparison with that of the bulk counterpart Ge (299 cm^{-1}), respectively. With regard to the microstructure of heterostructural nanowires, the downshift of the LO mode may be caused by tensile stress, which affects the Raman line by a downshift. And the different shift scales are attracted by the different sizes of the Ge subnanowires and Ge nanocrystalline [8].

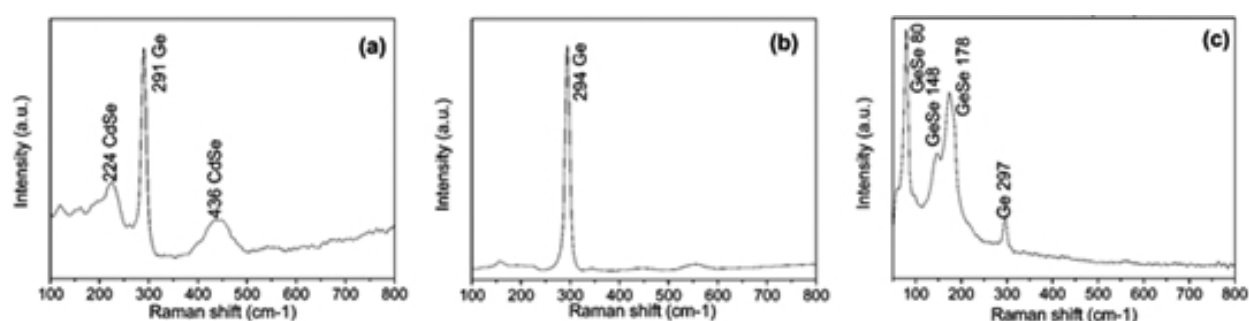


Figure 7. Raman spectrum of (a) CdSe-Ge biaxial nanowires and CdSe-Ge-CdSe triaxial nanowires. (b) CdSe-Ge biaxial nanowire core/polycrystalline Ge sheath heterostructures. (c) Ge-GeSe biaxial heterostructure nanowires.

The individual layer in SnS_2 is known as an S-Sn-S sandwich bonded unit. Each Sn atom is octahedrally coordinated with six nearest neighbor sulfur atoms, while each S atom is nested at the top of a triangle of Sn atoms. The sandwich layers in the elementary cell occur along the c axis and bonded together by Vander Waals forces. The normal modes of vibration in SnS_2 are given by the irreducible representations of the D_{3d} point group at the center of the Brillouin zone: $\Gamma = A_{1g} + E_g + 2A_{2u} + 2E_{2u}$. Two Raman-active modes (A_{1g} and E_g) and two IR-active modes (A_{2u} and E_u) are found. In view of the existence of an inversion center, the IR- and Raman-active modes are mutually exclusive. On the other hand, six atoms in the unit cell of SnS_2 extend over two sandwich layers. Eighteen normal vibration modes can be represented by the following irreducible form: $\Gamma = 3A_1 + 3B_1 + 3E_1 + 3E_2$. Based on the analysis above, there are six modes, which are both IR- and Raman-active, belonging to A_1 and E_1 , and three Raman-active modes belonging to E_2 . The B_1 modes are silent, while the three acoustic modes belong to A_1 and E_1 [9].

The RS of β - SnS_2 nanocrystal is illustrated in our former work [10]. The spectra show one first-order peak at 312 cm^{-1} that corresponding to A_{1g} mode. The RS of as-prepared SnS_2 shows a slight redshift in comparison with that of bulk materials (peak at 317 cm^{-1}). The redshift of phonon peaks is due to spatial confinement of phonon modes. The first-order E_g mode (peak

at 208 cm⁻¹) cannot be observed, which likely results from a nanosize effect. A wide peak between 450 and 750 cm⁻¹, which only observed in the bulk materials at lower temperature, may be attributed to second-order effects.

The phonon dispersion of single-layer MoS₂ has three acoustic and six optical branches derivatized from the nine vibrational modes at the Γ point. The three acoustic branches are the in-plane longitudinal acoustic (LA), the transverse acoustic (TA), and the out-of-plane acoustic (ZA) modes. The six optical branches are two in-plane longitudinal optical (LO₁ and LO₂), two in-plane transverse optical (TO₁ and TO₂), and two out-of-plane optical (ZO₁ and ZO₂) branches.

For 2L and bulk MoS₂, there are 18 phonon branches, which are split from nine phonon branches in 1LMoS₂. The phonon dispersions of 1L and bulk MoS₂ are very similar, except for the three new branches below 100 cm⁻¹ in bulk because of interlayer vibrations. There are similar optical phonon dispersion curves for 1L, 2L, and bulk MoS₂ because of the weak Vander Waals interlayer interactions in 2L and bulk MoS₂ [11].

Raman spectroscopy is also used to accurately identify the layer number of MoS₂. The frequency difference between out-of-plane A_{1g} and in-plane E_{2g}¹ mode of MoS₂ is denoted as $\Delta\omega$. From monolayer to bulk MoS₂, $\Delta\omega$ monotonically increases from 19.57 cm⁻¹ to 25.5 cm⁻¹. In our work [12], two strong peak at ~ 379 cm⁻¹ and ~ 402 cm⁻¹ can be assigned as in-plane E_{2g}¹ mode and out-of-plane A_{1g} mode of MoS₂, respectively, which has a redshift in comparison with that of the bulk MoS₂. The $\Delta\omega$ is about 23 cm⁻¹, indicating that the as-grown MoS₂ contains tri-layer MoS₂.

The phonon dispersion and density-of-states curves along the principal symmetry directions of kesterite CZTS were calculated using a density functional theory by Khare et al. [13]. The phonon states around 50–160 cm⁻¹ are mainly composed of vibrations of the three metal cations with some contribution from the sulfur anions. The phonon states around 250–300 cm⁻¹ are mainly composed of vibrations of the Zn cations and S anions with some contribution from the Cu cations. The phonon states from 310 to 340 cm⁻¹ are mainly a result of vibrations of S anions, whereas those from 340 to 370 cm⁻¹ are composed of the vibrations of Sn cations and S anions.

To more exactly confirm secondary phases in Cu₂-II-IV-VI₄ semiconductors, Raman scattering studies have been extensively performed. From the vibrational point of view, the zone-center phonon representation of the kesterite structure space group $\bar{I}4$ is constituted of 21 optical modes: $\Gamma = 3A + 6B + 6E_1 + 6E_2$, where 12B, E₁, and E₂ modes are infrared active, whereas 15A, B, E₁, and E₂ modes are Raman active. According to our work [14], the single peak at about 328 cm⁻¹ of Raman spectrum of the as-prepared CZTS nanocrystals can be assigned to breathing mode of sulfur atoms around metal ions in CZTS. Moreover, Raman spectrum of CZTS has about 8 cm⁻¹ redshifts compared with that of the responding bulk counterpart which may be due to a smaller size effect.

In our work of fabrication of Cu₂ZnSn_xSe_{4-x} solid solution nanocrystallines [15], RS revealed that vibrating modes were modulated by x -values. The peak position of 170, 189, and 229 cm⁻¹ shifted to higher frequency with increasing x -value in CZTSSe, respectively. Those peaks

completely disappeared when $x = 4$. Moreover, a wide peak located at about 330 cm^{-1} appeared when $x > 0$ and the relative intensity increased with increasing x -value. Such results indicate that Se elements were gradually replaced by S elements in CZTSSe solid solution system.

Acknowledgements

This work was supported by the National Natural Science Foundation of China under Grant Nos. 11174049 and 61376017.

Author details

Lin Sun, Lingcong Shi and Chunrui Wang*

*Address all correspondence to: crwang@dhu.edu.cn

Department of Applied Physics, Donghua University, Shanghai, China

References

- [1] Xu, J., Wang, C., Wu, B., Xu, X., Chen, X., Oh, H., Baek, H., & Yi, G. C. Twinning effect on photoluminescence spectra of ZnSe nanowires. *Journal of Applied Physics*. 2014;116(17):174303. doi:10.1063/1.4900850.
- [2] Xu, J., Wang, C., Lu, A., Wu, B., Chen, X., Oh, H., Baek, H., Yi, G., & Ouyang, L. Photoluminescence of excitons and defects in ZnSe-based longitudinal twinning nanowires. *Journal of Physics D: Applied Physics*. 2014;47(48):485302. doi:10.1088/0022-3727/47/48/485302.
- [3] Xu, J., Lu, A., Wang, C., Zou, R., Liu, X., Wu, X., Wang, Y., Li, S., Sun, L., Chen, X., Oh, H., Baek, H., Yi, G., & Chu, J. ZnSe-based longitudinal twinning nanowires. *Advanced Engineering Materials*. 2014;16(4):459–465. doi:10.1002/adem.201300405.
- [4] Zhang, G. et al. *Lattice Vibration Spectroscopy*. Beijing: Higher Education Press; 2001
- [5] Huang, K., & Han, R. *Solid-State Physics*. Beijing: Higher Education Press; 1988.
- [6] Strocio, M. A., & Dutta, M. *Phonons in Nanostructures*. Cambridge: Cambridge University Press; 2005.
- [7] Wang, H. *Luminescence and vibrating properties of Zn-based group II-VI nanostructures*. Master's thesis. Donghua University. 2012.

- [8] Cai, J. Controllable synthesis and vibrating properties of CdSe based heterostructure nanowires. Master's thesis. Donghua University. 2011.
- [9] Smith, A. J., Meek, P. E., & Liang, W. Y. Raman scattering studies of SnS₂ and SnSe₂. *Journal of Physics C: Solid State Physics*. 1977;10(8):1321. doi:10.1088/0022-3719/10/8/035.
- [10] Wang, C. Synthesis and properties of iodine and sulfide nanomaterials. PhD thesis. University of Science and Technology of China. 2002.
- [11] Zhang, X., Qiao, X. F., Shi, W., Wu, J. B., Jiang, D. S., & Tan, P.H. Phonon and Raman scattering of two-dimensional transition metal dichalcogenides from monolayer, multilayer to bulk material. *Chemical Society Reviews*. 2015;44(9):2757–2785. doi:10.1039/C4CS00282B.
- [12] Fu, Y. Fabrication and properties of ZnO/CdS/MoS₂ heterostructure nanorod arrays. Master's thesis. Donghua University. 2016.
- [13] Khare, A., Himmetoglu, B., Johnson, M., Norris, D. J., Cococcioni, M., & Aydil, E. S. Calculation of the lattice dynamics and Raman spectra of copper zinc tin chalcogenides and comparison to experiments. *Journal of Applied Physics*. 2012;111(8):083707. doi:10.1063/1.4704191.
- [14] Wang, C., Cheng, C., Cao, Y., Fang, W., Zhao, L., & Xu, X. Synthesis of Cu₂ZnSnS₄ nanocrystallines by a hydrothermal route. *Japanese Journal of Applied Physics*. 2011;50(6R):065003. doi:10.1143/JJAP.50.065003.
- [15] Cao, Y.. Fabrication and characterization of Cu₂ZnSnS_xSe_{4-x} thin film solar cell absorber layer material. Master's thesis, Donghua University. 2012

IntechOpen

IntechOpen

IntechOpen